Cell Reports
Physical Science

CellPress
OPEN ACCESS

Article

Dynamical and thermodynamical origins of motility-induced phase separation

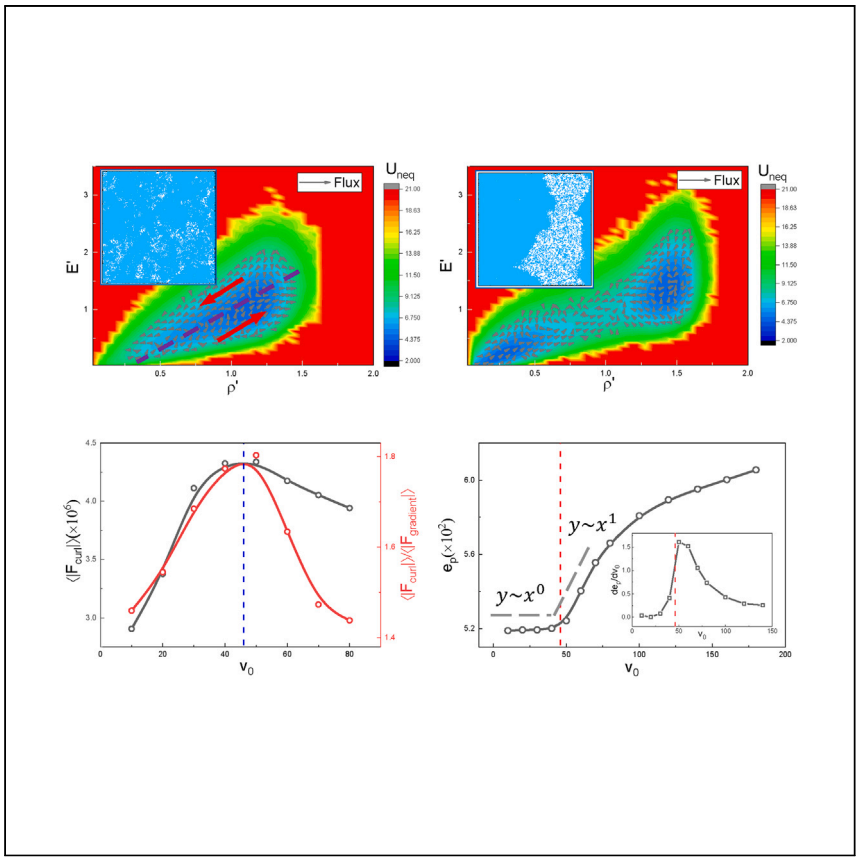

Su et al. introduce a coarse-grained mapping method to probe detailed balance breaking in the density-energy phase space, which can be used to reveal the dynamical and thermodynamical origins of motility-induced phase separation based on the nonequilibrium potential and flux landscape theory.

Jie Su, Zhiyu Cao, Jin Wang, Huijun Jiang, Zhonghuai Hou

jin.wang.1@stonybrook.edu (J.W.)
hjjiang3@ustc.edu.cn (H.J.)
hzhlj@ustc.edu.cn (Z.H.)

Highlights

The nonequilibrium flux is the dynamical origin of MIPS

The transition of the scaling behavior of EPR is the thermodynamical origin of MIPS

The EPR's transition point provides a new way to confirm the phase boundary of MIP

Su et al., Cell Reports Physical Science 5, 101817
February 21, 2024
https://doi.org/10.1016/j.xcrp.2024.101817

Please cite this article in press as: Su et al., Dynamical and thermodynamical origins of motility-induced phase separation, Cell Reports Physical Science (2024), https://doi.org/10.1016/j.xcrp.2024.101817

Cell Reports
Physical Science

CellPress
OPEN ACCESS

Article

Dynamical and thermodynamical origins of motility-induced phase separation

Jie Su,[1,3,5] Zhiyu Cao,[1,5] Jin Wang,[4,*] Huijun Jiang,[1,2,*] and Zhonghuai Hou[1,2,6,*]

SUMMARY

Active matter systems are inherently out of equilibrium and break the detailed balance (DB) at the microscopic scale, exhibiting vital collective phenomena such as motility-induced phase separation (MIPS). Here, we introduce a coarse-grained mapping method to probe DB breaking in the density-energy phase space, which allows us to reveal the dynamical and thermodynamical origins of MIPS based on the landscape-flux theory. Hallmarks of nonequilibrium properties are manifested by identifying the visible steady-state probability flux in the coarse-grained phase space. Remarkably, the flux of the system with activity lower than the MIPS threshold has the tendency to split the single potential well of the uniform-density phase and generate two wells of phases with different densities, demonstrating that the nonequilibrium flux is the dynamical origin of MIPS. Moreover, we find that the entropy production rate shows a transition of scaling behavior around the MIPS threshold, providing an indicator for the thermodynamical origin of MIPS.

INTRODUCTION

Active matter widely exists in various scales of nature, ranging from microscopic and mesoscopic swimmers such as bacteria and the active Janus spheres to macroscopic objects such as fish, birds, and horses.[1,2] Since the active systems break the detailed balance (DB) at the microscopic scale, they cannot be described by equilibrium statistical mechanics, and the nonequilibrium dynamics may manifest as curl flux in a phase space of mesoscopic coordinates.[3–10] In comparison to their passive counterparts, active systems exhibit many novel dynamical behaviors, such as the emergence of dynamic chirality,[11–14] functional self-assembly,[15–18] and abundant collective motions such as vortex, swarm,[18–22] and the particularly well-known motility-induced phase separation (MIPS).[23] It has been observed that particles with pure repulsion can spontaneously undergo phase separation between dense and dilute fluid phases when the activity is higher than a certain threshold. The unique nonequilibrium properties of MIPS have attracted tremendous research interests.[23–48]

It is well known that some physical properties of equilibrium systems have singularities at the transition point, such as the discontinuous enthalpy change in the first-order transition or the discontinuous change in heat capacity in the second-order transition.[49] Nevertheless, it is quite difficult to define state functions of nonequilibrium systems, such as Gibbs free energy, so it is very important but challenging to figure out the underlying mechanism of MIPS by other means. Previously, the self-trapping effect of active particles was proposed by Cates et al. to understand the mechanism of MIPS.[23] That is, active particles tend to accumulate where they move more slowly and will slow down at high density, which then creates positive feedback and further

[1]Hefei National Research Center for Physical Sciences at the Microscale & Key Laboratory of Precision and Intelligent Chemistry, University of Science and Technology of China, Hefei, Anhui 230026, China

[2]Hefei National Laboratory, University of Science and Technology of China, Hefei 230088, China

[3]Center for Theoretical Interdisciplinary Sciences, Wenzhou Institute, University of Chinese Academy of Sciences, Wenzhou 325001, China

[4]Department of Chemistry and of Physics and Astronomy, State University of New York of Stony Brook, Stony Brook, NY 11794, USA

[5]These authors contributed equally

[6]Lead contact

*Correspondence:
jin.wang.1@stonybrook.edu (J.W.),
hjjiang3@ustc.edu.cn (H.J.),
hzhlj@ustc.edu.cn (Z.H.)

https://doi.org/10.1016/j.xcrp.2024.101817

Please cite this article in press as: Su et al., Dynamical and thermodynamical origins of motility-induced phase separation, Cell Reports Physical Science (2024), https://doi.org/10.1016/j.xcrp.2024.101817

leads to MIPS.[23,24] This mechanism provides a basic physical picture for investigating the occurrence of MIPS but cannot provide a deep understanding of MIPS, such as confirming the phase boundary or the type of phase transition. Therefore, a series of theoretical analyses are performed to explore the underlying mechanism of MIPS on the basis of the self-trapping effect, including not only studies taking the perspective of dynamical mechanisms, such as the kinetic model,[25–27] but also works starting from the view of thermodynamical ones, for instance swim pressure,[28–30] scalar φ^4 field theory,[44,45] effective Cahn-Hilliard equation,[46–48] and renormalization group.[50,51] Also, the statistical analysis for thermodynamical quantities of numerics can provide new insights into MIPS.[52,53] However, it remains unclear how broken DB propagates from particle-scale dynamics to large-scale collective dynamics in active matter systems, and the connection to the dynamical and thermodynamical origins of MIPS.

In this work, we introduce a constructive method mapping the real space, including motions of active particles into a low-dimensional phase space with two dimensions of local particle density and local particle energy. In the coarse-grained phase space, the theoretical approach of nonequilibrium potential and flux landscape theory, which is widely used in nonequilibrium systems such as gene regulatory circuit motifs, cell cycle, population dynamics and ecology, etc.,[54–59] is applied to explore the dynamical and thermodynamical origins of MIPS. By using this approach, on the one hand, we can establish the nonequilibrium potential landscape of the active system, which reflects global information such as the phase states and their weights. The nonequilibrium potential has only one potential well when the active system is in a single phase, while it has two wells corresponding to dilute and dense phases when MIPS occurs. On the other hand, the nonequilibrium curl flux as well as the entropy production rate (EPR) can also be obtained by this approach. Since nonequilibrium flux induced by self-propulsion can be decomposed from the driving force of the system while the EPR is related to the time-reversal symmetry (TRS) breaking and apparent dissipation on certain scale (density-energy space), they can be used to explore the dynamical and thermodynamical natures and changes of the active system during the MIPS process. As a result, the obtained nonequilibrium potential has only one potential well (representing the single phase) for activity before the MIPS threshold. Interestingly, we find that the flux inside the well tends to push local states of low density to be increasingly lower and those of higher density to be increasingly higher. In other words, the nonequilibrium curl flux favors global movements instead of localizing in one point in the state space so that it can generate a tearing force to split the potential well (the single phase) to create new wells of different densities (MIPS), rather than the gradient force tending to localize the state around the attractor, demonstrating that the nonequilibrium flux is the dynamical origin of the occurrence of MIPS. Further analysis reveals that the contribution of the nonequilibrium flux depends nonmonotonically on particle activity and shows a maximum splitting effect at the MIPS threshold. Moreover, it is observed that the obtained EPR is nearly unchanged before the threshold and that it increases rapidly as activity increases after the threshold. The transition of the scaling behavior of EPR on activity might be considered as the thermodynamical origin of MIPS, and the transition point can be used to confirm the phase boundary of MIPS.

RESULTS AND DISCUSSION

Coarse-grained mapping method

We propose a constructive method mapping the real space including motions of active particles into a low-dimensional coarse-grained phase space with two

Please cite this article in press as: Su et al., Dynamical and thermodynamical origins of motility-induced phase separation, Cell Reports Physical Science (2024), https://doi.org/10.1016/j.xcrp.2024.101817

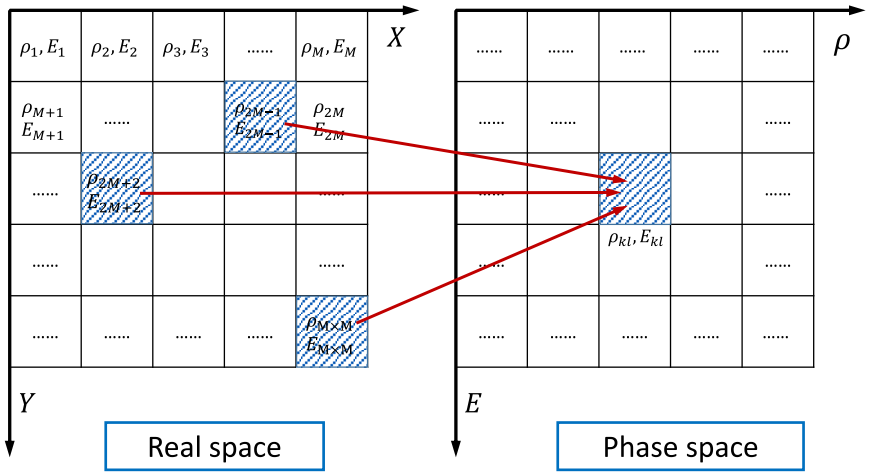

Figure 1. Schematic of the coarse-grained mapping from the evolution of cells in real space to that in the $\rho - E$ phase space

As an example, if the three blue cells located at different positions in the real space have the same ρ and E, then they will be mapped into the same cell with $\rho_{kl} = \rho$ and $E_{kl} = E$ in the phase space.

dimensions of local particle density and local particle energy as follows. For N spherical active Brownian particles (ABPs) of diameter σ, mass m, and friction coefficient γ in a quasi-two-dimensional space with size L and periodic boundary conditions, the motion of the i-th ABP located at $\mathbf{r}_i$ obeys the following Langevin equations[37,40,60]:

$$m\ddot{\mathbf{r}}_i = -\gamma\dot{\mathbf{r}}_i + \gamma v_0 \mathbf{n}_i - \sum_{j=1, j\neq i}^{N} \nabla_{\mathbf{r}_i} U(r_{ij}) + \boldsymbol{\xi}_i, \qquad \text{(Equation 1)}$$

$$J\ddot{\theta}_i = -\gamma_r \dot{\theta}_i + \zeta_i. \qquad \text{(Equation 2)}$$

Herein, v_0 and $\mathbf{n}_i = (\cos\theta_i, \sin\theta_i)$ are the amplitude and direction of active speed, respectively, with θ_i being the angle of $\mathbf{n}_i$. $\mathbf{r}_{ij} = \mathbf{r}_i - \mathbf{r}_j$ is the vector pointing from the j-th ABP to the i-th ABP, and r_{ij} is its norm. The interaction between a pair of ABPs is described by the purely repulsive Weeks-Chandler-Andersen potential, $U(r_{ij}) = 4\epsilon[(\sigma/r_{ij})^{12} - (\sigma/r_{ij})^6 + 1/4]$ for $r_{ij} < 2^{1/6}\sigma$ and $U(r_{ij}) = 0$ otherwise, where ϵ is the interaction strength. $\boldsymbol{\xi}_i$ and ζ_i denote the random force in the form of independent Gaussian white noises with time correlations $\langle\boldsymbol{\xi}_i(t)\boldsymbol{\xi}_j(t')\rangle = 2\gamma^2 D_t \mathbf{I}\delta_{ij}\delta(t-t')$ and $\langle\zeta_i(t)\zeta_j(t')\rangle = 2\gamma_r^2 D_r \delta_{ij}\delta(t-t')$, where $\mathbf{I}$ is the unit matrix, $D_t = k_B T/\gamma$ is the translation diffusion coefficient with k_B as the Boltzmann constant and T as the temperature, and $D_r = k_B T/\gamma_r$ is the rotational diffusion coefficient, with $\gamma_r = \sigma^2\gamma/3$ being the rotational friction coefficient. $J = \sigma^2 m/10$ denotes the moment of inertia, which couples with the mass and diameter of the spherical ABP.

Based on the motion equations, Equations 1 and 2, we divide the real space into $M\times M$ cells with size $a\times a$ ($M = L/a$) as shown in Figure 1 (left). In the i-th cell, two coarse-grained variables, local particle density and local total energy, can then be calculated as $\rho_i(t) = n_i/a^2$, where n_i is the number of particles in the i-th cell and $E_i(t) = \sum_{q\in cell_i} 0.5 m \mathbf{v}_q^2(t)$, where $\mathbf{v}_q(t)$ is the speed of the q-th ABP in the i-th cell. Similarly, the density-energy ($\rho - E$) space can also be divided into cells with steps $\delta\rho$ along the ρ dimension and δE along the E dimension (Figure 1, right). Then, the i-th cell in real space can be mapped into the (k,l) cell in $\rho - E$ space if $\rho_i(t) \in [k\delta\rho, (k+1)\delta\rho)$ and $E_i(t) \in [l\delta E, (l+1)\delta E)$ at time t. If there are different cells

Please cite this article in press as: Su et al., Dynamical and thermodynamical origins of motility-induced phase separation, Cell Reports Physical Science (2024), https://doi.org/10.1016/j.xcrp.2024.101817

in the real space of the same $\rho(t)$ and $E(t)$, they will be mapped into the same cell in $\rho - E$ space (blue cells in Figure 1). As shown as an example in Figure 1, if the three blue cells have the same ρ_i and E_i located at different places in the real space, then they will be mapped into the same cell with $\rho_{kl} = \rho_i$ and $E_{kl} = E_i$ in the phase space so that the probability of the blue cell in the $\rho - E$ phase space is $P(\rho_{kl}, E_{kl}, t) = 3/M^2$. Hence, the probability distribution $P(\rho, E, t)$ in the $\rho - E$ phase space can then be calculated. For convenience, variables ρ and E with one subscript denote the local density and local energy of cells in real space, respectively, and those with two subscripts are those of cells in $\rho - E$ space in follows, if not otherwise stated.

As will be proven later, the density-energy phase space is sufficiently coarse grained, where the non-Markovity of active matter systems does not manifest at such scale. Hence, the nonequilibrium dynamics of each cell in the $\rho - E$ phase space can be written as

$$\dot{\rho}_{kl}(t) = F_\rho(\rho_{kl}, E_{kl}) + \xi_\rho(\rho_{kl}, E_{kl}, t) \quad \text{(Equation 3)}$$

$$\dot{E}_{kl}(t) = F_E(\rho_{kl}, E_{kl}) + \xi_E(\rho_{kl}, E_{kl}, t). \quad \text{(Equation 4)}$$

Herein, $\dot{\rho}_{kl}(t)$ and $\dot{E}_{kl}(t)$ are calculated by averaging over mapping cells in real space. F_ρ and F_E are the deterministic "driving forces" with $F_\rho(\rho_{kl}, E_{kl}) = \langle \dot{\rho}_{kl}(t) \rangle$ and $F_E(\rho_{kl}, E_{kl}) = \langle \dot{E}_{kl}(t) \rangle$ ($\langle \cdot \rangle$ denotes time averaging when the system reaches the steady state). ξ_ρ and ξ_E are the stochastic terms with time correlations $\langle \boldsymbol{\xi}(\rho_{kl}, E_{kl}, t) \boldsymbol{\xi}(\rho_{kl}, E_{kl}, t') \rangle = 2\mathbf{D}(\rho_{kl}, E_{kl}) \delta(t - t')$, where $\boldsymbol{\xi}$ is a vector including the components of ξ_ρ and ξ_E and $\mathbf{D}(\rho_{kl}, E_{kl})$ is a 2×2 diffusion coefficient tensor consisting of $D_{\rho\rho}$, $D_{\rho E}$, $D_{E\rho}$, and D_{EE}. This diffusion coefficient tensor can be obtained by the Fourier transform of the time-correlation functions of the stochastic term $\boldsymbol{\xi}$. More details can be found in the supplemental information. The power spectrum functions for $v_0 = 100$ are shown in Figure S1 as an example, which proves that ξ_ρ and ξ_E are white noises, demonstrating that the dynamics of the active system in the $\rho - E$ phase space is indeed Markovian.

Nonequilibrium potential and flux in the density-energy space

Based on our coarse-grained mapping method, both the probability distribution $P(\rho, E, t)$ and the dynamical equation of cells (Equations 3 and 4) in the $\rho - E$ phase space can be obtained from the numerical simulations of active systems. We then apply the nonequilibrium potential and flux theory[54–59] to figure out the dynamical and thermodynamical origins of MIPS in the density-energy phase space (more details can be found in the supplemental information).

When the active system reaches the steady state, the probability distribution $P(\rho, E, t)$ is unchanged over time, i.e., $\partial P_{ss}(\rho, E, t)/\partial t = 0$ (the subscript ss denotes the steady state). The effective nonequilibrium potential U_{neq} can then be defined naturally as $U_{neq}(\rho, E) = -\ln P_{ss}(\rho, E)$. According to the Fokker-Planck equation, it is known that $\partial P/\partial t = -\nabla \cdot \mathbf{J}(t)$. When the system is in equilibrium, the flux $\mathbf{J} = 0$ so that the driving force only depends on the gradient of the effective potential, i.e., $\mathbf{F} = (F_\rho, F_E)^{\mathrm{T}} = -\mathbf{D} \cdot \nabla U$ (the superscript T denotes the transpose of a matrix). However, when the system is in nonequilibrium, the flux $\mathbf{J}$ can exist in the form of a rotational curl or, more precisely, a recurrent field,[54–59] and the steady-state nonequilibrium flux $\mathbf{J}_{ss}(\mathbf{x})$ with $\mathbf{x} = (\rho, E)^{\mathrm{T}}$ can be described as $\mathbf{J}_{ss}(\mathbf{x}) = \mathbf{F}(\mathbf{x}) P_{ss}(\mathbf{x}) - \nabla_{\mathbf{x}} \cdot [\mathbf{D} P_{ss}(\mathbf{x})]$. Here, the driving force $\mathbf{F}$ no longer depends solely on the gradient of the nonequilibrium potential U_{neq} because the steady-state flux field $\mathbf{J}_{ss}$ contributes to $\mathbf{F}$. Therefore, $\mathbf{F}$ can be decomposed into the gradient part ($\mathbf{F}_{gradient}$), the curl one ($\mathbf{F}_{curl}$), and the one related to the spatial dependent noise

Please cite this article in press as: Su et al., Dynamical and thermodynamical origins of motility-induced phase separation, Cell Reports Physical Science (2024), https://doi.org/10.1016/j.xcrp.2024.101817

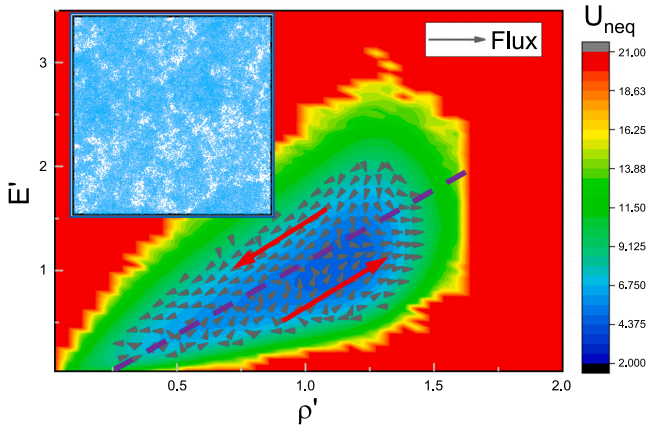

Figure 2. The nonequilibrium potential and flux landscape of the active system with $v_0 = 40$

The nonequilibrium potential is presented as the colored background, and the flux field is shown as the black arrows. The purple line is the division line of the flux direction, and the red arrows represent the whole flux direction of each segment. The inset is a typical snapshot in the steady state.

$(\mathbf{F}_D)$, $\mathbf{F}(\mathbf{x}) = \mathbf{F}_{gradient}(\mathbf{x}) + \mathbf{F}_{curl}(\mathbf{x}) + \mathbf{F}_D(\mathbf{x}) = -\mathbf{D}\cdot\nabla U_{neq}(\mathbf{x}) + \mathbf{v}_{ss}(\mathbf{x}) + \nabla\cdot\mathbf{D}$ (in Ito's representation, $\nabla\cdot\mathbf{D}$ represents the divergence of the diffusion tensor[54]). Here, $\mathbf{v}_{ss}(\mathbf{x}) = \mathbf{J}_{ss}(\mathbf{x})/P_{ss}(\mathbf{x})$ is the local flow or velocity in steady states.[61]

Combining our coarse-grained mapping method with the nonequilibrium potential and flux theory, it is convenient to analyze the dynamical and thermodynamical properties of MIPS in density-energy phase space based on numerical simulations in real space. In simulations, σ and k_BT are basic units for length and energy, respectively, and $\gamma = 1.0$ so that the basic unit for time is $\gamma\sigma^2/(k_BT)$. Notice that previous researches on MIPS have usually focused on the mesoscopic active systems and that the models are overdamped due to the low Reynolds number of the system; hence, we set $m = 10^{-5}$ to reach the overdamped limit.[37] We fix $L = 200$, $\epsilon = 10.0$, and $N = 30,720$ so that the averaged number density becomes $\rho_0 = N/L^2 = 0.768$ and the volume fraction is $\varphi_0 = \pi\sigma^2\rho_0/4 = 0.6$. Active systems with such a volume fraction will undergo phase transition from the single phase to the coexisting phase at a threshold around $v_0 = 50$. We first run simulations from a random initial configuration for a long time, $t_1 = 500$, with the time step $\Delta t = 10^{-6}$ to ensure that the system reaches the steady state and then perform the simulations for another long amount of time, $t_2 = 500$, to attain the steady-state evolution of ABPs. In the following, the data of local density and local energy are rescaled by ρ_0 and the averaged local energy E_0, i.e., $\rho' = \rho/\rho_0$ and $E' = E/E_0$.

Dynamical origin of MIPS

Firstly, we focus on the dynamics of the active system just before the MIPS threshold. As an example, the nonequilibrium potential of the active system with $v_0 = 40$ in the $\rho' - E'$ phase space is presented in Figure 2. It can be observed that there is only one potential well representing a single phase without any phase-separation behaviors, which agrees with the typical snapshot shown in the inset of Figure 2. Moreover, the obtained flux field is further presented as the black arrows in Figure 2, where the nonzero flux demonstrates that the DB at the coarse-grained scale is broken. More interestingly, it can be found that the flux located inside the potential well can be explicitly divided into two parts with opposite directions. For a given E', the flux located in the region with small ρ' (on the left side of the purple dashed line in Figure 2) tends to push the local state to the negative direction of ρ', rendering

Please cite this article in press as: Su et al., Dynamical and thermodynamical origins of motility-induced phase separation, Cell Reports Physical Science (2024), https://doi.org/10.1016/j.xcrp.2024.101817

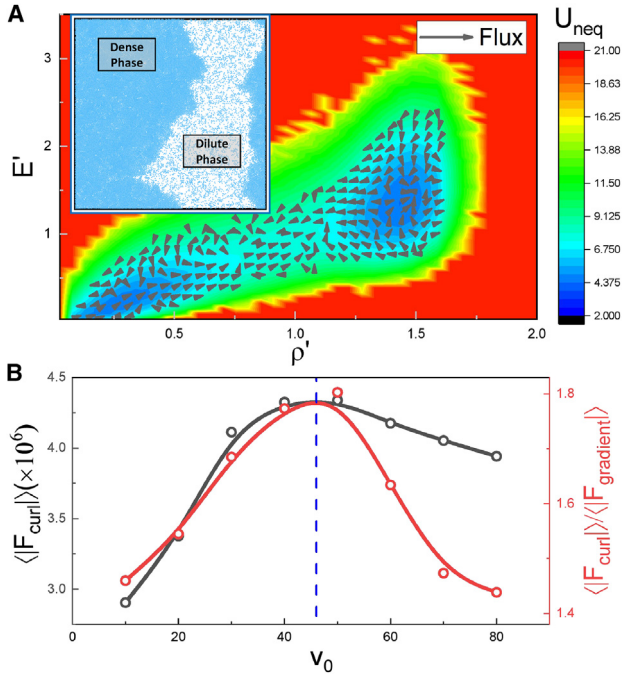

Figure 3. The landscape and flux after the MIPS threshold and the flux's contribution

(A) The nonequilibrium potential (colored background) and flux (black arrows) of the active system with $v_0 = 100$. The inset is a typical snapshot in the steady state.

(B) Dependence of $\langle|\mathbf{F}_{curl}|\rangle$ and $\langle|\mathbf{F}_{curl}|\rangle/\langle|\mathbf{F}_{gradient}|\rangle$ on v_0. The dashed blue line denotes the MIPS threshold.

ρ' to be increasingly lower. The flux located in the region with large ρ' (on the right side of the purple dashed line) prefers to push the local state to the positive direction of ρ', leading to increasingly higher ρ'. From another view of a given ρ', the flux points to the lower ρ' direction when E' is large (above the purple dashed line), while the flux points to the higher ρ' direction when E' is small (below the purple dashed line). This means that the local state with high density or small average single-particle energy will be pushed to the higher ρ' direction by the nonequilibrium flux field, which is consistent with the self-trapping mechanism of MIPS proposed by Cates et al.[23] As mentioned, the driving force for the nonequilibrium dynamics can be decomposed into the gradient force of the landscape and the curl flux force. While the gradient force tends to attract the system down to the point attractor and stabilize it, the curl flux that breaks the DB is rotational. Thus, the rotational force tends to create flows rather than localizing at a point state. Therefore, the dynamical effect of the flux is to destabilize the point attractor state while stabilizing the continuous flow in the state space. In short, the nonequilibrium flux field consisting of two parts with opposite directions tries to split the potential well to create new wells with different densities. Therefore, we hold the view that the nonequilibrium flux force is the dynamical origin of MIPS.

Next, the dynamics after MIPS occurs (such as $v_0 = 100$) is considered. As presented in Figure 3A, it can be observed that the nonequilibrium potential has two potential wells with different ρ', where the potential well located at small ρ' represents the dilute phase and the one located at large ρ' denotes the dense phase, consistent with the typical snapshot shown in the inset of Figure 3A. In addition, it is found that the flux rotates in a counterclockwise direction between these two potential wells. It is noted that for the equilibrium phase separation

Please cite this article in press as: Su et al., Dynamical and thermodynamical origins of motility-induced phase separation, Cell Reports Physical Science (2024), https://doi.org/10.1016/j.xcrp.2024.101817

without any nonequilibrium flux, particles in one of the potential wells have a very difficult time jumping into the other one with just the sole help of noise. However, particles can be easily pushed from one phase to the other due to the nonequilibrium flux in active systems, which is consistent with the observations in simulations.

To quantitatively characterize the splitting effect induced by the nonequilibrium flux in the MIPS process, we calculate the absolute value of the nonequilibrium flux and its relative value to the driving force due to nonequilibrium potential as the functions of activity v_0, that is, the curl part $\langle|\mathbf{F}_{curl}|\rangle$ as well as the ratio of the curl part to the gradient one $\langle|\mathbf{F}_{curl}|\rangle/\langle|\mathbf{F}_{gradient}|\rangle$, which can be calculated by $\langle|\mathbf{F}_{curl}|\rangle = \iint|\mathbf{J}_{ss}/P_{ss}|d\rho dE$, and $\langle|\mathbf{F}_{gradient}|\rangle = \iint|\mathbf{D}\cdot\nabla U_{neq}|d\rho dE$. The integral bounds of ρ is set to be $[0.5, 0.95]$ because only the flux located inside the regions with the density between the dense and dilute phases contributes to the formation of MIPS. The dependence of $\langle|\mathbf{F}_{curl}|\rangle$ and $\langle|\mathbf{F}_{curl}|\rangle/\langle|\mathbf{F}_{gradient}|\rangle$ on v_0 is illustrated in Figure 3B. It can be found that both $\langle|\mathbf{F}_{curl}|\rangle$ (black symbols and line) and $\langle|\mathbf{F}_{curl}|\rangle/\langle|\mathbf{F}_{gradient}|\rangle$ (red symbols and line) depend nonmonotonically on v_0 and show maximal values around the MIPS threshold, indicating that the splitting effect induced by the nonequilibrium flux reaches its maximum when MIPS occurs.

Thermodynamical origin of MIPS

Now, we focus on the thermodynamics of MIPS. To quantify DB breaking and TRS in the density-energy phase space, we introduce the noise-averaged global EPR e_p in the steady states[61]:

$$\begin{aligned} e_p &= \iint \frac{\mathbf{J}_{ss}^{\mathrm{T}}(\rho,E)\cdot\mathbf{D}^{-1}(\rho,E)\cdot\mathbf{J}_{ss}(\rho,E)}{P_{ss}(\rho,E)}d\rho dE \\ &= \iint \mathbf{v}_{ss}^{\mathrm{T}}(\rho,E)\cdot\mathbf{D}^{-1}(\rho,E)\cdot\mathbf{v}_{ss}(\rho,E)P_{ss}(\rho,E)d\rho dE. \end{aligned} \quad \text{(Equation 5)}$$

The obtained e_p dependent on the particle activity v_0 is shown in Figure 4A. It can be found that e_p increases monotonically as v_0 increases, indicating that higher activity will bring more dissipation into the system, further making the system far away from the equilibrium. More interestingly, it can be observed that e_p scales differently on v_0 before and after the MIPS threshold. When v_0 is lower than the threshold, e_p remains nearly unchanged. However, once v_0 exceeds the threshold, e_p increases linearly, with a slope of approximately 1. To take a closer look at this transition, the obtained derivative of e_p dependent on v_0 is illustrated in the inset of Figure 4A. Clearly, de_p/dv_0 holds slightly higher than 0 before the MIPS threshold (the dashed red line) and rapidly becomes very large when v_0 passes the threshold. Actually, de_p/dv_0 quantifies the change of irreversibility/apparent EP by varying the order parameter (activity), i.e., how much the irreversibility of the system changes as the ability of the active monomers to absorb energy from the environment improves. This slope being 0 means that as the monomer's ability to absorb energy increases, the system does not become more irreversible on an apparent scale. On the other hand, when this slope is 1, the system becomes more irreversible. Since the steady-state flux is mainly contributed by the E component of the local flow (see the supplemental information and Figure S2 for details), the net transition in the energy space dominates the scaling behavior and sharpness of EP.

The thermodynamical origin of MIPS can be attributed to the sharp transition of scaling behavior of the EP in the density-energy phase space. From the expression of the EP, it is directly related to the flux measuring the degree of DB breaking. The flux thus forms the dynamical basis of the nonequilibrium thermodynamical cost. Since there is a steep change of nonequilibrium thermodynamical cost

Please cite this article in press as: Su et al., Dynamical and thermodynamical origins of motility-induced phase separation, Cell Reports Physical Science (2024), https://doi.org/10.1016/j.xcrp.2024.101817

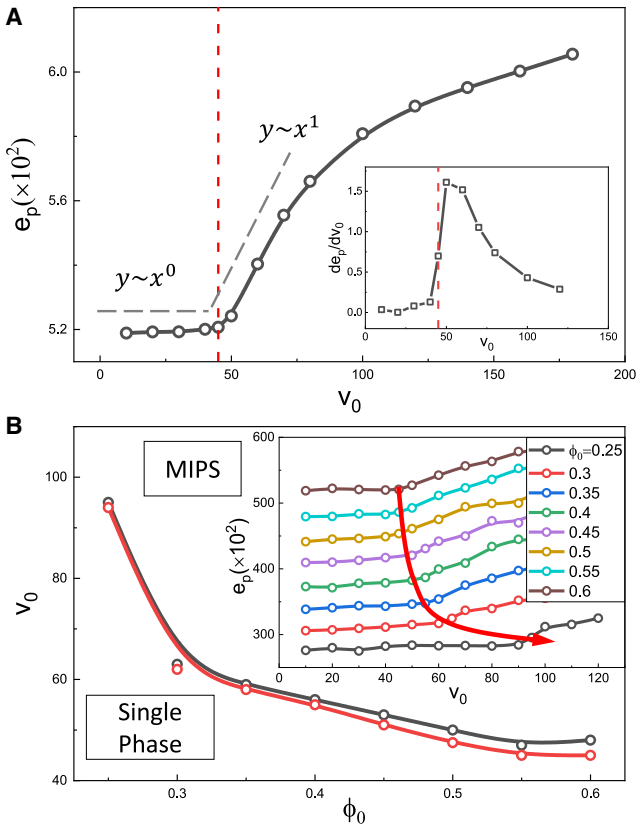

Figure 4. The thermodynamical origin of MIPS

(A) Dependence of the entropy production rate e_p on v_0. The dashed lines denote functions of scales 0 and 1. The inset is the dependence of the derivative of e_p on v_0. The dashed red lines denote the MIPS threshold.

(B) The phase diagram of MIPS results from the direct simulation (the black symbols and line) and the transition of EPR's scaling behavior (the red symbols and line). The inset is the dependence of e_p on v_0 for varying φ_0, and the red arrow presents the shift of the EPR's transition point as v_0 decreases.

characterized by EPR when the MIPS system transforms from a single phase (one attractor basin) to phase separation with two coexisting phases (two attractor basins), it provides an indicator that the EPR serves as the thermodynamical origin of MIPS. We believe that the significant change in behavior of the EP can be explained as follows. On the one hand, the distribution of EP may violate the large deviation principle, which has been found to be closely associated with dynamical phase transitions.[62,63] This behavior of EP has been widely observed in active systems,[64] albeit not always in the form of MIPS but rather significant changes in dynamical behavior, such as dynamic arrest in smaller EP systems and the emergence of collective behavior in larger ones.[65] Similarly, this also implies an interplay between structure and dissipation.[66,67] On the other hand, this sudden increase in EP may come from the fact that the maintenance cost of two attractor landscapes is usually higher than that of a single-basin landscape. In other words, switching from a single-basin landscape to a two-basin landscape requires significant flux force to split the one-basin landscape and form the two-basin landscape. In addition, this observation provides a reliable tool to identify the MIPS threshold between the single and coexisting phases, which confirms that the phase-transition point can be characterized in terms of EP,[68–72] especially in active matter

Please cite this article in press as: Su et al., Dynamical and thermodynamical origins of motility-induced phase separation, Cell Reports Physical Science (2024), https://doi.org/10.1016/j.xcrp.2024.101817

systems.[73–75] For example, Caballero et al.[76,77] utilized active scalar φ^4 theories to study the behavior of EP near the phase-separation critical point, showing that the singular part of the EPR remains finite or itself diverges, while the critical scaling for EP ranks among universal dynamic Ising-class properties. In addition, Shim et al., based on a Vicsek-like model, studied the EP during the ordered-disordered phase-transition point, showing that the EP of particles disappears in the disordered phase, while in the ordered phase, the EP follows critical scaling laws and becomes positive.[73] Herein, the EP we calculated is in a particular density-energy space to reflect the DB breaking and TRS breaking on this scale. Particularly, the scaling exponent of EP we found is similar to the results in Shim et al.,[73] which may indicate that our coarse-graining strategy can capture important natures related to active matter phase transitions. Therefore, compared to the other studies focusing on the EP of active matter,[64–66,78–89] our findings provide fresh insights into the origin of MIPS.

In order to provide a more direct verification of the accuracy and validity of our approach, the phase diagram with the coexistence curve is obtained by our method (Figure 4B). Based on the additional simulation results, the dependence of e_p on v_0 for varying φ_0 is illustrated in the inset of Figure 4B. It is found that as the volume fraction φ_0 decreases, the transition point of the EPR's scaling behavior shifts to the larger v_0 (the red arrow). According to these transition points, the obtained coexistence curve is shown as the red line in Figure 4B, which is almost overlapped with the one resulting from the direct simulation (the black line). This result not only demonstrates that the EPR's transition point can be used to confirm the phase boundary of MIPS but also provides the verification that the thermodynamical origin of MIPS is attributed to the transition of EPR's scaling behavior.

In summary, we found the density-energy phase space by using the coarse-grained mapping method, which is suitable and clear to characterize the dynamical and thermodynamical origins of MIPS. By applying the nonequilibrium potential and flux landscape theory, not only can the nonequilibrium potential landscape of the active system, which reflects global information such as phase states and their weights, be established, but also the nonequilibrium curl flux as well as the EPR can be obtained and used to explore the dynamical and thermodynamical natures and changes of the active system during the MIPS process. Our method can provide another perspective on MIPS compared with the effective equilibrium approach. It is found that the nonequilibrium flux with opposite directions tends to split the single nonequilibrium potential well before the MIPS threshold. This not only demonstrates directly that the nonequilibrium flux is the dynamical origin of the occurrence of MIPS but also provides evidence that the DB is significantly broken at the coarse-grained scale. In addition, intensive simulations reveal that the EPR shows a transition of scaling behavior around the MIPS threshold, which not only serves as the thermodynamical origin of MIPS but also provides a new way to confirm the phase boundary of MIPS. Our findings bring new insights and propose a new route to understand the nonequilibrium nature of MIPS.

EXPERIMENTAL PROCEDURES

Resource availability

Lead contact

Further information and requests for resources should be directed to and will be fulfilled by the lead contact, jin.wang1@stonybrook.edu Zhonghuai Hou (hzhlj@ustc.edu.cn).

Please cite this article in press as: Su et al., Dynamical and thermodynamical origins of motility-induced phase separation, Cell Reports Physical Science (2024), https://doi.org/10.1016/j.xcrp.2024.101817

Materials availability

No new materials were generated in this study.

Data and code availability

All study data are included in this article and/or the supplemental information. Any additional information required is available from the lead contact upon request.

Model Building

We started with the Langevin equations of the active Brownian particles (ABPs) model and attained the steady-state evolution of ABPs by numerical simulations. Based on the coarse-grained mapping method, the motions of ABPs in the real space can be mapped into the density-energy phase space. Finally, by applying the nonequilibrium potential and flux theory, we can figure out the dynamical and thermodynamical origins of MIPS. Details of models and methods are provided in the supplemental experimental procedures.

SUPPLEMENTAL INFORMATION

Supplemental information can be found online at https://doi.org/10.1016/j.xcrp.2024.101817.

ACKNOWLEDGMENTS

J.S., Z.C., H.J., and Z.H. are supported by MOST (2022YFA1303100), NSFC (32090040, 21973085, 21833007, and 22373090), and the Fundamental Research Funds for the Central Universities (WK2340000104).

AUTHOR CONTRIBUTIONS

Z.H. and J.W. conceived the idea and designed the research. H.J. provided the model and supervised the research. J.S. performed the simulations and data analysis. Z.C. provided the theoretical analysis. All authors discussed the results and cowrote the manuscript.

DECLARATION OF INTERESTS

The authors declare no competing interests.

Received: June 30, 2023
Revised: December 19, 2023
Accepted: January 16, 2024
Published: February 5, 2024

REFERENCES

1. Bechinger, C., Di Leonardo, R., Löwen, H., Reichhardt, C., Volpe, G., and Volpe, G. (2016). Active particles in complex and crowded environments. Rev. Mod. Phys. *88*, 045006.

2. Vicsek, T., and Zafeiris, A. (2012). Collective motion. Phys. Rep. *517*, 71–140.

3. Battle, C., Broedersz, C.P., Fakhri, N., Geyer, V.F., Howard, J., Schmidt, C.F., and MacKintosh, F.C. (2016). Broken detailed balance at mesoscopic scales in active biological systems. Science *352*, 604–607.

4. Gnesotto, F.S., Mura, F., Gladrow, J., and Broedersz, C.P. (2018). Broken detailed balance and non-equilibrium dynamics in living systems: a review. Rep. Prog. Phys. *81*, 066601.

5. Gladrow, J., Fakhri, N., MacKintosh, F.C., Schmidt, C.F., and Broedersz, C.P. (2016). Broken detailed balance of filament dynamics in active networks. Phys. Rev. Lett. *116*, 248301.

6. Mura, F., Gradziuk, G., and Broedersz, C.P. (2018). Nonequilibrium scaling behavior in driven soft biological assemblies. Phys. Rev. Lett. *121*, 038002.

7. Seara, D.S., Yadav, V., Linsmeier, I., Tabatabai, A.P., Oakes, P.W., Tabei, S.M.A., Banerjee, S., and Murrell, M.P. (2018). Entropy production rate is maximized in non-contractile actomyosin. Nat. Commun. *9*, 4948.

8. Gladrow, J., Broedersz, C.P., and Schmidt, C.F. (2017). Nonequilibrium dynamics of probe filaments in actin-myosin networks. Phys. Rev. E *96*, 022408.

9. Dieball, C., and Godec, A. (2022). Mathematical, thermodynamical, and experimental necessity for coarse graining empirical densities and currents in continuous space. Phys. Rev. Lett. *129*, 140601.

10. Dieball, C., and Godec, A. (2022). Coarse graining empirical densities and currents in continuous-space steady states. Phys. Rev. Research *4*, 033243.

11. DiLuzio, W.R., Turner, L., Mayer, M., Garstecki, P., Weibel, D.B., Berg, H.C., and Whitesides, G.M. (2005). Escherichia coli swim on the right-hand side. Nature *435*, 1271–1274.

12. Riedel, I.H., Kruse, K., and Howard, J. (2005). A self-organized vortex array of hydrodynamically entrained sperm cells. Science *309*, 300–303.

13. Kümmel, F., ten Hagen, B., Wittkowski, R., Buttinoni, I., Eichhorn, R., Volpe, G., Löwen, H., and Bechinger, C. (2013). Circular motion of asymmetric self-propelling particles. Phys. Rev. Lett. *110*, 198302.

14. Gibbs, J.G., Kothari, S., Saintillan, D., and Zhao, Y.-P. (2011). Geometrically designing the kinematic behavior of catalytic nanomotors. Nano Lett. *11*, 2543–2550.

15. Mallory, S.A., and Cacciuto, A. (2019). Activity-enhanced self-assembly of a colloidal kagome lattice. J. Am. Chem. Soc. *141*, 2500–2507.

16. Gou, Y., Jiang, H., and Hou, Z. (2019). Assembled superlattice with dynamic chirality in a mixture of biased-active and passive particles. Soft Matter *15*, 9104–9110.

17. Du, Y., Jiang, H., and Hou, Z. (2019). Self-assembly of active core corona particles into highly ordered and self-healing structures. J. Chem. Phys. *151*, 154904.

18. Yan, J., Han, M., Zhang, J., Xu, C., Luijten, E., and Granick, S. (2016). Reconfiguring active particles by electrostatic imbalance. Nat. Mater. *15*, 1095–1099.

19. Sumino, Y., Nagai, K.H., Shitaka, Y., Tanaka, D., Yoshikawa, K., Chaté, H., and Oiwa, K. (2012). Large-scale vortex lattice emerging from collectively moving microtubules. Nature *483*, 448–452.

20. Jiang, H., Ding, H., Pu, M., and Hou, Z. (2017). Emergence of collective dynamical chirality for achiral active particles. Soft Matter *13*, 836–841.

21. Karani, H., Pradillo, G.E., and Vlahovska, P.M. (2019). Tuning the random walk of active colloids: From individual run-and-tumble to dynamic clustering. Phys. Rev. Lett. *123*, 208002.

22. Gou, Y.-liang, Jiang, H.-jun, and Hou, Z.-huai (2020). Emergent swarming states in active particles system with opposite anisotropic interactions. Chi. J. Chem. Phys. *33*, 717–726.

23. Tailleur, J., and Cates, M.E. (2008). Statistical mechanics of interacting run-and-tumble bacteria. Phys. Rev. Lett. *100*, 218103.

24. Cates, M.E., and Tailleur, J. (2015). Motility-induced phase separation. Annu. Rev. Condens. Matter Phys. *6*, 219–244.

25. Redner, G.S., Hagan, M.F., and Baskaran, A. (2013). Structure and dynamics of a phase-separating active colloidal fluid. Phys. Rev. Lett. *110*, 055701.

26. Redner, G.S., Baskaran, A., and Hagan, M.F. (2013). Reentrant phase behavior in active colloids with attraction. Phys. Rev. E *88*, 012305.

27. Redner, G.S., Wagner, C.G., Baskaran, A., and Hagan, M.F. (2016). Classical nucleation theory description of active colloid assembly. Phys. Rev. Lett. *117*, 148002.

28. Takatori, S.C., Yan, W., and Brady, J.F. (2014). Swim pressure: Stress generation in active matter. Phys. Rev. Lett. *113*, 028103.

29. Takatori, S.C., and Brady, J.F. (2015). Towards a thermodynamics of active matter. Phys. Rev. E *91*, 032117.

30. Patch, A., Yllanes, D., and Marchetti, M.C. (2017). Kinetics of motility-induced phase separation and swim pressure. Phys. Rev. E *95*, 012601.

31. Fily, Y., Henkes, S., and Marchetti, M.C. (2014). Freezing and phase separation of self-propelled disks. Soft Matter *10*, 2132–2140.

32. Stenhammar, J., Marenduzzo, D., Allen, R.J., and Cates, M.E. (2014). Phase behaviour of active brownian particles: the role of dimensionality. Soft Matter *10*, 1489–1499.

33. Zöttl, A., and Stark, H. (2014). Hydrodynamics determines collective motion and phase behavior of active colloids in quasi-two-dimensional confinement. Phys. Rev. Lett. *112*, 118101.

34. Furukawa, A., Marenduzzo, D., and Cates, M.E. (2014). Activity-induced clustering in model dumbbell swimmers: The role of hydrodynamic interactions. Phys. Rev. E *90*, 022303.

35. Blaschke, J., Maurer, M., Menon, K., Zöttl, A., and Stark, H. (2016). Phase separation and coexistence of hydrodynamically interacting microswimmers. Soft Matter *12*, 9821–9831.

36. Stenhammar, J., Wittkowski, R., Marenduzzo, D., and Cates, M.E. (2015). Activity-induced phase separation and self-assembly in mixtures of active and passive particles. Phys. Rev. Lett. *114*, 018301.

37. Mandal, S., Liebchen, B., and Löwen, H. (2019). Motility-induced temperature difference in coexisting phases. Phys. Rev. Lett. *123*, 228001.

38. Siebert, J.T., Letz, J., Speck, T., and Virnau, P. (2017). Phase behavior of active brownian disks, spheres, and dimers. Soft Matter *13*, 1020–1026.

39. Liao, G.-J., and Klapp, S.H.L. (2018). Klapp. Clustering and phase separation of circle swimmers dispersed in a monolayer. Soft Matter *14*, 7873–7882.

40. Su, J., Jiang, H., and Hou, Z. (2021). Inertia-induced nucleation-like motility-induced phase separation. New J. Phys. *23*, 013005.

41. Du, Y., Jiang, H., and Hou, Z. (2020). Rod-assisted heterogeneous nucleation in active suspensions. Soft Matter *16*, 6434–6441.

42. Caprini, L., Marini Bettolo Marconi, U., and Puglisi, A. (2020). Spontaneous velocity alignment in motility-induced phase separation. Phys. Rev. Lett. *124*, 078001.

43. Caprini, L., Marconi, U.M.B., Maggi, C., Paoluzzi, M., and Puglisi, A. (2020). Hidden velocity ordering in dense suspensions of self-propelled disks. Phys. Rev. Research *2*, 023321.

44. Wittkowski, R., Tiribocchi, A., Stenhammar, J., Allen, R.J., Marenduzzo, D., and Cates, M.E. (2014). Scalar φ4field theory for active-particle phase separation. Nat. Commun. *5*, 4351.

45. Tjhung, E., Nardini, C., and Cates, M.E. (2018). Cluster phases and bubbly phase separation in active fluids: Reversal of the ostwald process. Phys. Rev. X *8*, 031080.

46. Speck, T., Bialké, J., Menzel, A.M., and Löwen, H. (2014). Effective cahn-hilliard equation for the phase separation of active brownian particles. Phys. Rev. Lett. *112*, 218304.

47. Speck, T., Menzel, A.M., Bialké, J., and Löwen, H. (2015). Dynamical mean-field theory and weakly non-linear analysis for the phase separation of active brownian particles. J. Chem. Phys. *142*, 224109.

48. Rapp, L., Bergmann, F., and Zimmermann, W. (2019). Systematic extension of the cahn-hilliard model for motility-induced phase separation. Eur. Phys. J. E *42*, 57.

49. Lev Davidovich Landau, and Lifshitz, E.M. (2013). Statistical Physics*volume 5* (Elsevier).

50. Maggi, C., Gnan, N., Paoluzzi, M., Zaccarelli, E., and Crisanti, A. (2022). Critical active dynamics is captured by a colored-noise driven field theory. Commun. Phys. *5*, 55.

51. Caballero, F., Nardini, C., and Cates, M.E. (2018). From bulk to microphase separation in scalar active matter: a perturbative renormalization group analysis. J. Stat. Mech. *2018*, 123208.

52. Digregorio, P., Levis, D., Suma, A., Cugliandolo, L.F., Gonnella, G., and Pagonabarraga, I. (2018). Full phase diagram of active brownian disks: From melting to motility-induced phase separation. Phys. Rev. Lett. *121*, 098003.

53. Fily, Y., and Marchetti, M.C. (2012). Athermal phase separation of self-propelled particles with no alignment. Phys. Rev. Lett. *108*, 235702.

54. Wang, J., Xu, L., and Wang, E. (2008). Potential landscape and flux framework of nonequilibrium networks: robustness, dissipation, and coherence of biochemical oscillations. Proc. Natl. Acad. Sci. USA *105*, 12271–12276.

55. Li, C., and Wang, J. (2014). Landscape and flux reveal a new global view and physical quantification of mammalian cell cycle. Proc. Natl. Acad. Sci. USA *111*, 14130–14135.

56. Fang, X., Kruse, K., Lu, T., and Wang, J. (2019). Nonequilibrium physics in biology. Rev. Mod. Phys. *91*, 045004.

57. Chu, X., and Wang, J. (2020). Conformational state switching and pathways of chromosome dynamics in cell cycle. Appl. Phys. Rev. *7*, 031403.

58. Wang, J. (2015). Landscape and flux theory of non-equilibrium dynamical systems with application to biology. Adv. Phys. X. *64*, 1–137.

59. Fang, X., and Wang, J. (2020). Nonequilibrium thermodynamics in cell biology: Extending equilibrium formalism to cover living systems. Annu. Rev. Biophys. *49*, 227–246.

60. Löwen, H. (2020). Inertial effects of self-propelled particles: From active brownian to active langevin motion. J. Chem. Phys. *152*, 040901. 2020.

61. Seifert, U. (2012). Stochastic thermodynamics, fluctuation theorems and molecular machines. Rep. Prog. Phys. *75*, 126001.

62. Touchette, H. (2009). The large deviation approach to statistical mechanics. Phys. Rep. *478*, 1–69.

63. Jack, R.L. (2020). Ergodicity and large deviations in physical systems with stochastic dynamics. Eur. Phys. J. B *93*, 74.

64. Cagnetta, F., Corberi, F., Gonnella, G., and Suma, A. (2017). Large fluctuations and dynamic phase transition in a system of self-propelled particles. Phys. Rev. Lett. *119*, 158002.

65. Nemoto, T., Fodor, É., Cates, M.E., Jack, R.L., and Tailleur, J. (2019). Optimizing active work: Dynamical phase transitions, collective motion, and jamming. Phys. Rev. E *99*, 022605.

66. Tociu, L., Fodor, É., Nemoto, T., and Vaikuntanathan, S. (2019). How dissipation constrains fluctuations in nonequilibrium liquids: Diffusion, structure, and biased interactions. Phys. Rev. X *9*, 041026.

67. Nguyen, M., Qiu, Y., and Vaikuntanathan, S. (2021). Organization and self-assembly away from equilibrium: Toward thermodynamic design principles. Annu. Rev. Condens. Matter Phys. *12*, 273–290.

68. Crochik, L., and Tomé, T. (2005). Entropy production in the majority-vote model. Phys. Rev. E *72*, 057103.

69. Tomé, T., and Oliveira, Mário J de (2012). Entropy production in nonequilibrium systems at stationary states. Phys. Rev. Lett. *108*, 020601.

70. Noa, C.E.F., Harunari, P.E., de Oliveira, M.J., and Fiore, C.E. (2019). Entropy production as a tool for characterizing nonequilibrium phase transitions. Phys. Rev. E *100*, 012104.

71. Seara, D.S., Machta, B.B., and Murrell, M.P. (2021). Irreversibility in dynamical phases and transitions. Nat. Commun. *12*, 392–399.

72. Xiao, T.J., Hou, Z., and Xin, H. (2008). Entropy production and fluctuation theorem along a stochastic limit cycle. J. Chem. Phys. *129*, 114506.

73. Shim, P.S., Chun, H.-M., and Noh, J.D. (2016). Macroscopic time-reversal symmetry breaking at a nonequilibrium phase transition. Phys. Rev. E *93*, 012113.

74. Cao, Z., Su, J., Jiang, H., and Hou, Z. (2022). Effective entropy production and thermodynamic uncertainty relation of active brownian particles. Phys. Fluids *34*, 053310.

75. Xu, L., and Wang, J. (2020). Curl flux as a dynamical origin of the bifurcations/phase transitions of nonequilibrium systems: Cell fate decision making. J. Phys. Chem. B *124*, 2549–2559.

76. Caballero, F., and Cates, M.E. (2020). Stealth entropy production in active field theories near ising critical points. Phys. Rev. Lett. *124*, 240604.

77. Paoluzzi, M. (2022). Scaling of the entropy production rate in a φ 4 model of active matter. Phys. Rev. E *105*, 044139.

78. Fodor, É., Nardini, C., Cates, M.E., Tailleur, J., Visco, P., and Van Wijland, F. (2016). How far from equilibrium is active matter? Phys. Rev. Lett. *117*, 038103.

79. Mandal, D., Klymko, K., and DeWeese, M.R. (2017). Entropy production and fluctuation theorems for active matter. Phys. Rev. Lett. *119*, 258001.

80. Dabelow, L., Bo, S., and Eichhorn, R. (2019). Irreversibility in active matter systems: Fluctuation theorem and mutual information. Phys. Rev. X *9*, 021009.

81. Ganguly, C., and Chaudhuri, D. (2013). Stochastic thermodynamics of active brownian particles. Phys. Rev. E *88*, 032102.

82. Speck, T. (2016). Stochastic thermodynamics for active matter. Europhys. Lett. *114*, 30006.

83. Nardini, C., Fodor, É., Tjhung, E., Van Wijland, F., Tailleur, J., and Cates, M.E. (2017). Entropy production in field theories without time-reversal symmetry: quantifying the non-equilibrium character of active matter. Phys. Rev. X *7*, 021007.

84. Shankar, S., and Marchetti, M.C. (2018). Hidden entropy production and work fluctuations in an ideal active gas. Phys. Rev. E *98*, 020604.

85. Szamel, G. (2019). Stochastic thermodynamics for self-propelled particles. Phys. Rev. E *100*, 050603.

86. Crosato, E., Prokopenko, M., and Spinney, R.E. (2019). Irreversibility and emergent structure in active matter. Phys. Rev. E *100*, 042613.

87. Cao, Z., Jiang, H., and Hou, Z. (2021). Designing circle swimmers: Principles and strategies. J. Chem. Phys. *155*, 234901.

88. Guo, B., Ro, S., Shih, A., Trung, V Phan, Austin, R.H., Martiniani, S., Levine, D., and Paul, M.C. (2021). Play. Pause. Rewind. Measuring Local Entropy Production and Extractable Work in Active Matter. Preprint at arXiv. https://doi.org/10.48550/arXiv.2105.12707.

89. Bowick, M.J., Fakhri, N., Marchetti, M.C., and Ramaswamy, S. (2022). Symmetry, thermodynamics, and topology in active matter. Phys. Rev. X *12*, 010501.